

A lithium sulfonylimide COF-modified separator for high-performance Li-S batteries

Jie Liu^{1,3}, Jinping Zhang^{1,3}, Jie Zhu^{1,3}, Ruiqi Zhao^{1,3}, Yamin Zhang⁴, Yanfeng Ma^{1,3}, Chenxi Li^{1,3}, Hongtao Zhang^{1,3} (✉), and Yongsheng Chen^{1,2,3} (✉)

¹ The Centre of Nanoscale Science and Technology and Key Laboratory of Functional Polymer Materials, Institute of Polymer Chemistry, College of Chemistry, Nankai University, Tianjin 300071, China

² State Key Laboratory of Elemento-Organic Chemistry, Nankai University, Tianjin 300071, China

³ Renewable Energy Conversion and Storage Center (RECAST), Nankai University, Tianjin 300071, China

⁴ State Key Laboratory of Applied Organic Chemistry, College of Chemistry and Chemical Engineering, Lanzhou University, Lanzhou 730000, China

© Tsinghua University Press 2023

Received: 21 February 2023 / Revised: 12 March 2023 / Accepted: 21 March 2023

ABSTRACT

Lithium-sulfur (Li-S) batteries are highly regarded as the next-generation high-energy-density secondary batteries due to their high capacity and large theoretical energy density. However, the practical application of these batteries is hindered mainly by the polysulfide shuttle issue. Herein, we designed and synthesized a new lithium sulfonylimide covalent organic framework (COF) material (COF-LiSTFSI, LiSTFSI = lithium (4-styrenesulfonyl) (trifluoromethanesulfonyl)imide), and further used it to modify the common polypropylene (PP) separator of Li-S batteries. The COF-LiSTFSI with sulfonylimide anion groups features stronger electronegativity, thus can effectively facilitate the lithium ion conduction while significantly suppress the diffusion of polysulfides via the electrostatic interaction. Compared with the unmodified PP separator, the COF-LiSTFSI modified separator results in a high ionic conductivity ($1.50 \text{ mS}\cdot\text{cm}^{-1}$) and Li^+ transference number (0.68). Consequently, the Li-S battery using the COF-LiSTFSI modified separator achieves a high capacity of $1229.7 \text{ mAh}\cdot\text{g}^{-1}$ at 0.2 C and a low decay rate of only 0.042% per cycle after 1000 cycles at 1 C, compared with those of $941.5 \text{ mAh}\cdot\text{g}^{-1}$ and 0.061% using the unmodified PP separator, respectively. These results indicate that by choosing suitable functional groups, an effective strategy for COF-modified separators could be developed for high-performance Li-S batteries.

KEYWORDS

covalent organic frameworks, lithium sulfonylimide, ion selective, modified separator, lithium-sulfur batteries

1 Introduction

With the increasing demand for portable devices and electric vehicles, the development of high-energy-density secondary batteries has become highly urgent [1–3]. Although lithium-ion batteries as energy storage device have been widely commercialized, their energy density (approximately $387 \text{ Wh}\cdot\text{kg}^{-1}$) is relatively low and can hardly meet the ever-growing energy demands [4]. Benefiting from the characteristics of sulfur substance with high theoretical energy density ($2600 \text{ Wh}\cdot\text{kg}^{-1}$), environmental friendliness, natural abundance, and low cost, lithium-sulfur (Li-S) batteries offer great potentials for the next-generation energy storage systems [5]. However, during the long period of discharge/charge process, the incomplete reduction products of the sulfur cathode, known as lithium polysulfides (LiPSs), can dissolve in the electrolyte and move to the Li anode, resulting in the irreversible loss of active substances, which is known as the “shuttle effect” [6–8]. The shuttle effect can lead to rapid capacity fading and electrode structure destruction, which severely hinders the large-scale application of Li-S batteries [9, 10].

Numerous research studies have been carried out on resolving the notorious polysulfide shuttle effect, mainly by constructing

porous-structured host to anchor sulfur [11–13], utilizing novel electrolytes [14, 15], or developing modified separators to suppress polysulfide shuttling [16]. Among these strategies, separator modification is one of the most commonly explored approaches, as it provides a simple and efficient technology which is ideal for large-scale manufacturing and outperforms other laborious procedures. Although various materials such as carbon-based materials [17–19], polymers [20, 21], MXenes [22], metal compounds [23, 24], metal-organic frameworks [25, 26], and heterostructures [27] have been used to block the diffusion of polysulfides, some of them sacrifice the Li^+ diffusion when constructing the physical barrier for polysulfides shuttling, resulting in undesired transport resistance.

Covalent organic frameworks (COFs) are crystalline porous organic polymers with atomically precise building blocks linked by covalent bonds [28]. They possess low density, high surface area, robust structural stability, and homogeneously controllable nanopores, making them ideal for use as modified layers to block polysulfides [29, 30]. COFs with abundant lipophilic groups attached homogeneously on the aligned channels can also facilitate Li^+ diffusion. Sun et al. [31] developed lithiated covalent organic framework (Li-CON) nanosheets as a separator coating for high-

Address correspondence to Yongsheng Chen, yschen99@nankai.edu.cn; Hongtao Zhang, htzhang@nankai.edu.cn

performance Li-S batteries. The Li-CON had abundant lithiated sites that significantly reduced the diffusion barrier for fast lithium-ion transport. Wang et al. [32] designed and synthesized a dual-sulfonate COF with the concentrated sulfonic group, which acted as an ionic sieve for repelling polysulfide anions, adsorbing molecular LiPSs, and simultaneously facilitating Li⁺ migration. Furthermore, lithium sulfonylimide structures with high delocalization of negative charge and low Li⁺ dissociation energy are widely applied in single-ion conducting polymer electrolytes to promote Li⁺ transport [33].

Thus, by combining these two strategies together, it is believed that such COFs with lithium sulfonylimide group would not only promote Li⁺ transport but also suppress the shuttle effect when using them to modify the separator. Herein, we first designed and synthesized a novel ion selective covalent organic framework with lithium sulfonylimide group (denoted as COF-LiSTFSI, LiSTFSI = lithium (4-styrenesulfonyl) (trifluoromethanesulfonyl)imide) and then used it to modify the common polypropylene (PP) separator of Li-S batteries. This designed COF-LiSTFSI possesses abundant negative charged sulfonylimide groups capable of adsorbing molecular LiPSs and repelling polysulfide anions through electrostatic interaction, thus suppressing the shuttle effect. Furthermore, the sulfonylimide anion attached homogeneously on the aligned channels provides a highly ordered ion transportation pathway which significantly facilitates the Li⁺ transport. The COF-LiSTFSI modified separator results in an improved Li⁺ ionic conductivity of 1.50 mS·cm⁻¹ (from 0.20 mS·cm⁻¹ of PP separator) and Li⁺ transference number of 0.68 (from 0.29 of PP separator), indicating much improved facilitation of Li⁺ transport. The batteries assembled with COF-LiSTFSI modified separator deliver a high capacity of 1229.7 mAh·g⁻¹ at 0.2 C, and achieve a cycling of 1000 cycles at 1 C with a low decay rate of 0.042% per cycle, compared with those of 941.5 mAh·g⁻¹ and 0.061% when using the

commercial PP separator directly, respectively. In addition, when using a high loading sulfur cathode of 3.44 mg·cm⁻², a high capacity of 944.1 mAh·g⁻¹ at 0.2 C was achieved. These results indicate that by choosing suitable functional groups, an effective strategy for COF-modified separators could be developed for high-performance Li-S batteries.

2 Results and discussion

2.1 Synthesis and characterizations of COF-LiSTFSI

The COF-LiSTFSI was synthesized by a post-synthetic modification method as illustrated in Fig. 1(a). Initially, the methoxyl-functionalized COF (COF-OMe) was prepared by a Schiff base reaction between 1,3,5-tri-(4-aminophenyl)benzene (TPB) and 2,5-dimethoxy terephthalaldehyde (DMTP) [34]. Next, the COF-LiSTFSI was synthesized through Povarov (aza-Diels-Alder) reaction by grafting LiSTFSI into the COF-OMe. Prior to synthesizing COF-LiSTFSI, a model reaction of imine and LiSTFSI was carried out to confirm the feasibility of the Povarov reaction (Fig. 1(b)). The resulting model compound was confirmed by nuclear magnetic resonance (NMR) spectra (including ¹H NMR, ⁷Li NMR, and ¹⁹F NMR spectra, Figs. S1–S3 in the Electronic Supplementary Material (ESM)) and mass spectrometer (details are provided in Section S1 in the ESM), which demonstrated the feasibility of Povarov reaction and the integrity of lithium sulfonylimide group in the model compound. The schematic diagrams of the three-dimensional structure of the COF-OMe and COF-LiSTFSI are shown in Figs. 1(c) and 1(d).

The crystalline structures of both COF-OMe and COF-LiSTFSI were investigated by powder X-ray diffraction (PXRD) and theoretical structural simulations (Fig. 2(a) and Fig. S4 in the ESM). The PXRD analysis of COF-OMe displays characteristic

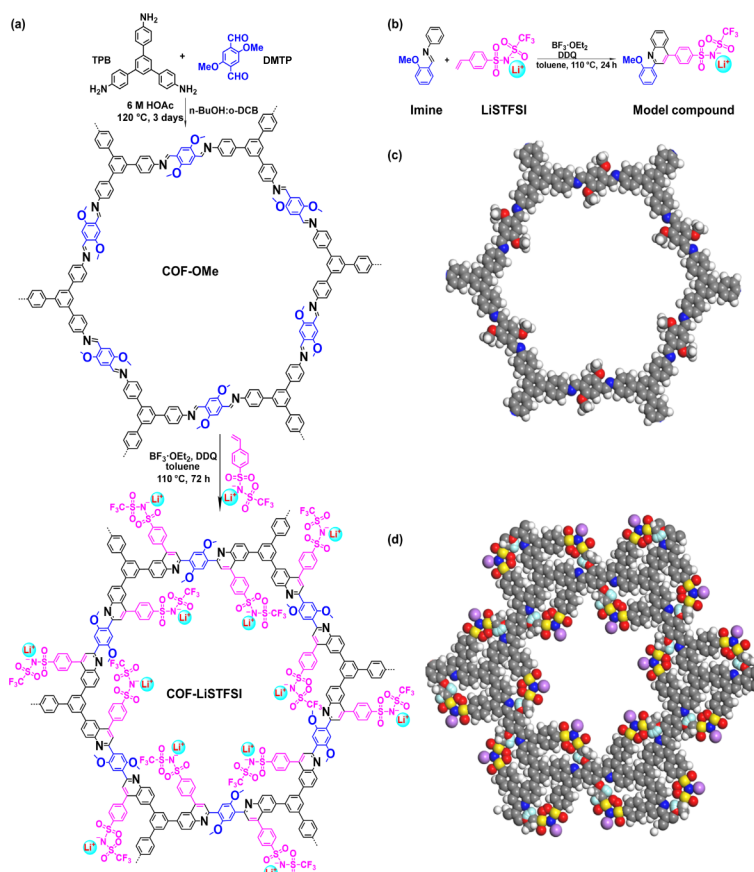


Figure 1 (a) Synthesis of COF-LiSTFSI by post-synthetic modification. (b) Synthesis of the model compound via Povarov reaction. (c) The schematic diagram of the three-dimensional structure of the COF-OMe. (d) The schematic diagram of the three-dimensional structure of the COF-LiSTFSI.

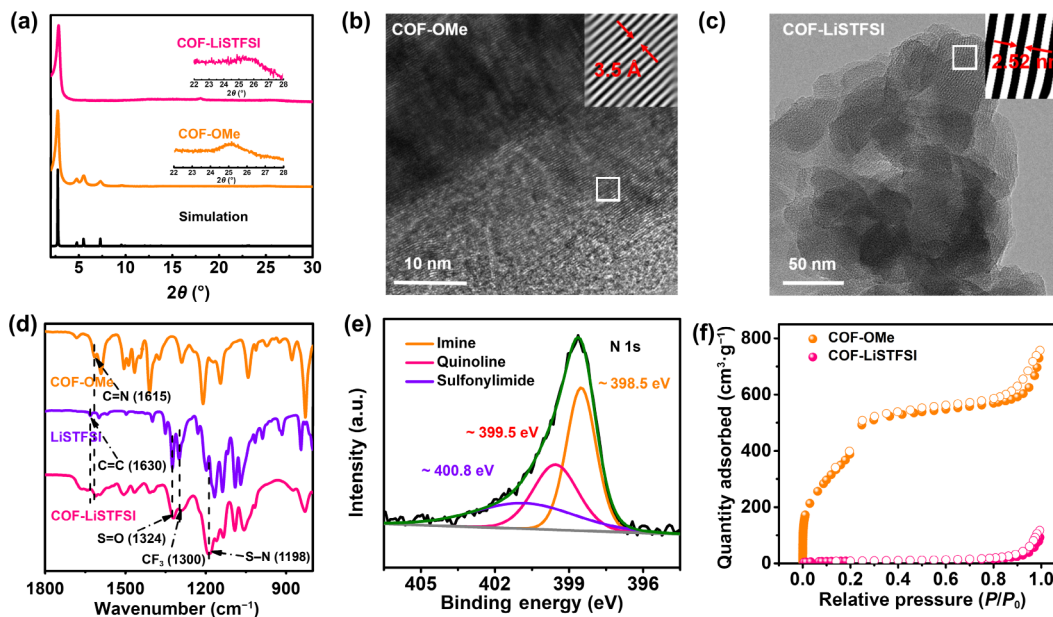


Figure 2 (a) PXRD patterns showing retention of crystallinity after the Povarov reaction. HRTEM characterizations of (b) COF-OMe and (c) COF-LiSTFSI. Insets are the Fourier-filtered images of the selected regions in the white squares. (d) FT-IR spectra. (e) N 1s XPS spectra of COF-LiSTFSI. (f) N₂ adsorption and desorption isotherms.

peaks consistent with the simulated PXRD results of the AA stacking pattern (the orange curve in Fig. 2(a)). The diffraction peaks at 2.74°, 4.78°, 5.54°, 7.32°, and 25.2° correspond to the (100), (110), (200), (210), and (001) facets, respectively, and can be clearly identified, indicating the high crystallinity of COF-OMe. After post-synthetic modification, the PXRD pattern of COF-LiSTFSI exhibits two prominent diffraction peaks at 2.84° and 25.7°, corresponding to the (100) and (001) facets, respectively (the pink curve in Fig. 2(a)). The crystallinity of COF-OMe and COF-LiSTFSI was further confirmed by high-resolution transmission electron microscopy (HRTEM). As shown in Fig. 2(b) and Fig. S5 in the ESM, the HRTEM images display distinct lattice fringes of COF-OMe with a *d*-spacing of 3.5 Å, which was consistent with the value obtained in PXRD (Fig. S4 in the ESM) and can be assigned to (001) facet of COF-OMe. Furthermore, the HRTEM images of COF-LiSTFSI (Fig. 2(c) and Fig. S6 in the ESM) also exhibit clear lattice fringes with a spacing of 2.52 nm, which matches well with the *d*-spacing of (100) facet measured by PXRD of COF-LiSTFSI. These results indicated that the crystallinity of COF-LiSTFSI was well maintained after the post-synthetic reaction.

The attachment of sulfonylimide group into COF-LiSTFSI was investigated through several analytical techniques. In Fig. 2(d), Fourier transform infrared (FT-IR) spectrum of COF-LiSTFSI shows new peaks at approximately 1324, 1300, and 1198 cm⁻¹ that correspond to the stretch vibrations of S=O, CF₃, and S-N (from the sulfonylimide group), respectively, which are not present in COF-OMe. Meanwhile, the quinolyl group (1594 and 1544 cm⁻¹) is also generated and the imine group (1615 cm⁻¹) of COF-OMe and C=C group (1630 cm⁻¹) of LiSTFSI disappeared (Fig. S9 in the ESM), which demonstrates that the sulfonylimide group was successfully connected onto COF-LiSTFSI. Solid-state ¹³C cross polarization magic angle spinning (CP-MAS) NMR spectroscopy also revealed the formation of the quinoline linkage of COF-LiSTFSI (Fig. S10 in the ESM). The COF-LiSTFSI sample shows the presence of 2-quinolyl carbon (152.5 ppm) and phenyl carbon (126.6 ppm), indicating the formation of quinolyl moiety. Furthermore, solid-state ¹⁹F CP-MAS NMR spectrum of COF-LiSTFSI (Fig. S11 in the ESM) shows a sharp peak at -77.6 ppm, which is consistent with the model compound and LiSTFSI (Fig. S3 in the ESM). X-ray photoelectron spectroscopy (XPS) analysis

was conducted to gain further insight into the connection of sulfonylimide. As shown in Fig. 2(e), the N 1s peaks at approximately 398.5, 399.5, and 400.8 eV in COF-LiSTFSI can be attributed to the imine, quinoline, and sulfonylimide N atoms, respectively. Based on the integration of the peak areas, the degree of LiSTFSI functionalization on the COF backbone was assessed to be around 41%. Additionally, the TEM elemental mapping images (Fig. S8 in the ESM) showed that both the fluorine and sulfur elements are evenly distributed in COF-LiSTFSI, thus indicating the successful introduction of the sulfonylimide group into COF-LiSTFSI. In addition, N₂ sorption analyses performed at 77 K revealed Brunauer-Emmett-Teller (BET) surface areas of 1514.8 and 68.5 m²·g⁻¹ for COF-OMe and COF-LiSTFSI, respectively (Fig. 2(f)). The decrease in specific surface area and pore size (Fig. S13 in the ESM) could be attributed to the incorporation of sulfonylimide group into the micropores.

2.2 Preparation, characterization, and properties of separators

Electrostatic potential distribution was calculated by density functional theory (DFT) method to investigate the surface charge of COF-OMe and COF-LiSTFSI (see details in Section S3 in the ESM). As shown in Fig. 3(a), the sulfonylimide group in COF-LiSTFSI exhibits intense electron density and strong electronegativity (indicated by the blue color region). The dipole moment value of COF-LiSTFSI (7.89 D) is larger than that of COF-OMe (2.64 D), demonstrating that the COF-LiSTFSI has a stronger polarity.

Zeta potential test was used to further confirm the surface charge property of COFs. As shown in Fig. 3(b), the COF-OMe has a value of -15.52 mV, while COF-LiSTFSI has a value of -55.84 mV, which indicates their electronegative nature. Accordingly, the COF-LiSTFSI with stronger electronegativity, which arises from the introduction of sulfonylimide group, could repel polysulfide anions through electrostatic repulsion interaction [32]. Additionally, as shown in Fig. 3(c), the stronger polarity of COF-LiSTFSI results in a higher binding energy when adsorbing LiPSs (-50.99 kcal·mol⁻¹) compared with COF-OMe (-40.04 kcal·mol⁻¹). This indicates that the COF-LiSTFSI modified separator might perform better adsorption LiPSs ability than COF-

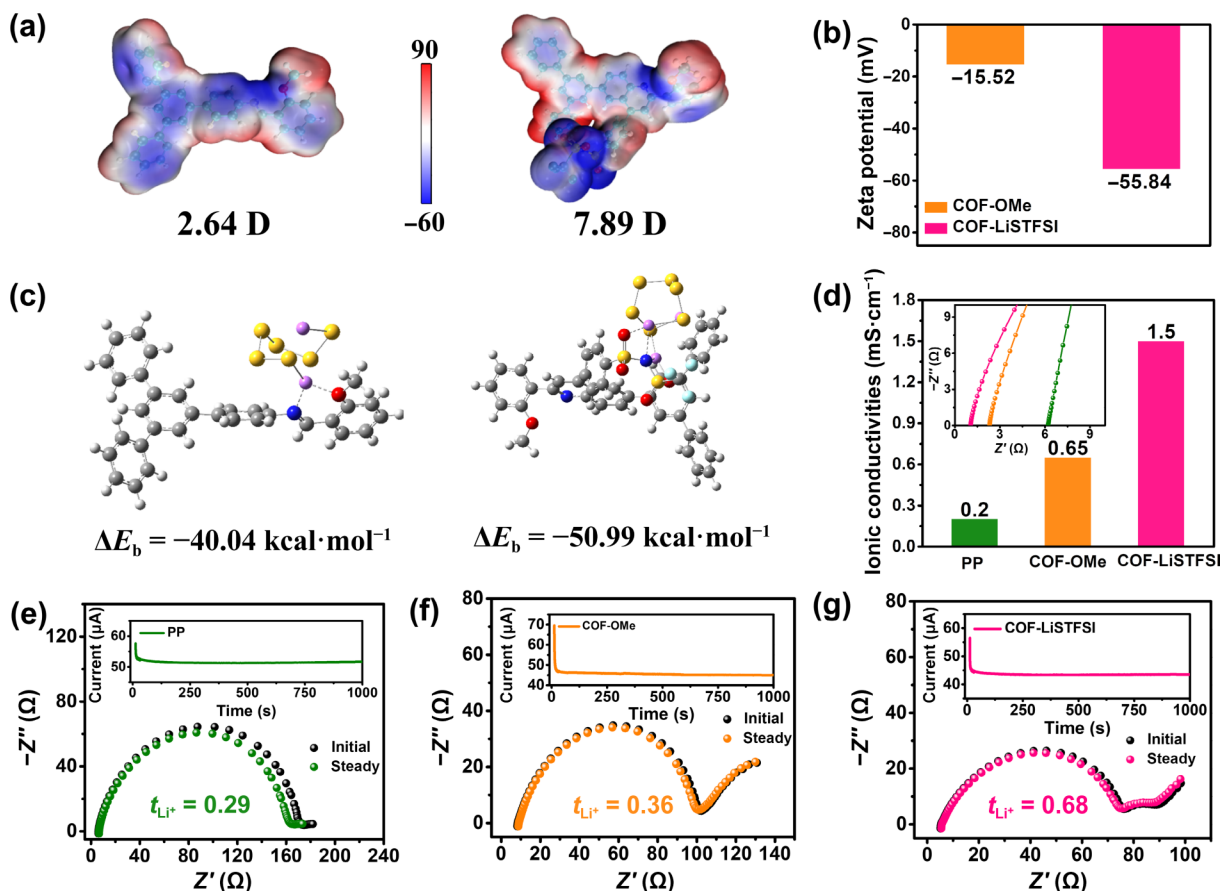


Figure 3 (a) Electrostatic potentials of the functional fragments of COF-Ome (left) and COF-LiSTFSI (right) (D is short for Debye). (b) Zeta potential values of COF-Ome and COF-LiSTFSI. (c) Interaction and binding energies between Li_2S_6 and the functional fragments of COF-Ome (left) and COF-LiSTFSI (right). (d) The ionic conductivities of PP, COF-Ome, and COF-LiSTFSI modified separators at 25 °C (inset: EIS plots). EIS plots of the symmetric cells of (e) PP, (f) COF-Ome, and (g) COF-LiSTFSI modified separators (insets are the chronoamperometric curves).

Ome. Electrolyte contact angle measurements were conducted to examine the electrolyte wettability of the PP, COF-Ome, and COF-LiSTFSI modified separators (Fig. S19 in the ESM). The corresponding contact angles were 29.69°, 15.59°, and 11.56°, respectively. The COF-LiSTFSI modified separator exhibits excellent electrolyte wettability due to the affinity between negatively charged sulfonylimide group of COF-LiSTFSI and polar molecules in the electrolyte. The excellent electrolyte wettability guarantees a high lithium ion migration rate. The physicochemical properties including ionic conductivity and Li^+ transference number of COF-modified separators were also evaluated. Specifically, the ionic conductivity of COF-LiSTFSI is determined to be 1.50 $\text{mS}\cdot\text{cm}^{-1}$, which is higher than that of COF-Ome (0.65 $\text{mS}\cdot\text{cm}^{-1}$) modified and the pristine PP (0.20 $\text{mS}\cdot\text{cm}^{-1}$) separators, respectively, indicating that the sulfonylimide group could enable efficient Li^+ conduction (Fig. 3(d)). Similar to the ionic conductivity, the COF-LiSTFSI modified separator exhibits a higher Li^+ transference number of 0.68 than that of COF-Ome (0.36) modified and the pristine PP (0.29) separators (Figs. 3(e)–3(g) and Table S1 in the ESM). This revealed that the COF-LiSTFSI modified separator possessed a superior capability for lithium ion selective conduction.

2.3 Electrochemical performance of Li-S batteries

The electrochemical properties of Li-S batteries with various separators were evaluated in a coin cell configuration, pairing the S/carbon black (CB) cathode (70% content, 0.8–1.2 $\text{mg}\cdot\text{cm}^{-2}$, see details in Section S1 in the ESM), the pristine PP or COF-modified separator, and Li anode. The electrochemical impedance spectroscopy (EIS) was used to analyze the electrochemical

kinetics and conductivity, with the Nyquist plots presented in Fig. 4(a). In comparison, the resistance of cell with COF-LiSTFSI modified separator is apparently much smaller than that of the pristine PP and COF-Ome modified separators, which proves the increased conductivity due to sulfonylimide functionalization. The cyclic voltammetry (CV) curves of the batteries at 0.1 $\text{mV}\cdot\text{s}^{-1}$ in the potential range of 1.7–2.8 V are shown in Fig. 4(b). In the cathodic scan, two peaks at around 2.3 and 2.0 V are attributed to reduction reaction of S_8 to high-order polysulfides (Li_2S_x , $x = 4\text{--}8$) and high-order polysulfides to $\text{Li}_2\text{S}/\text{Li}_2\text{S}_2$, respectively. In the anodic scan, the peak at around 2.4 V corresponds to the oxidation reaction of $\text{Li}_2\text{S}/\text{Li}_2\text{S}_2$ to S_8 [35]. The cell with COF-LiSTFSI modified separator presents the narrowest polarization voltage (0.31 V) compared with cells using the pristine PP and COF-Ome modified separators, further demonstrating the superior kinetics of redox conversion reactions. This was further confirmed by the first galvanostatic charge–discharge curves at 0.1 C (Fig. 4(c)), where the cell with COF-LiSTFSI modified separator shows a smaller polarization (0.18 V) compared with the cells using COF-Ome modified (0.20 V) and the pristine PP (0.26 V) separators, owing to the efficient lithium ion conduction of the COF-LiSTFSI coating. We also evaluated the CV curves of symmetric cells with Li_2S_6 -containing electrolyte. As shown in Fig. S21 in the ESM, the COF-LiSTFSI-based symmetric cell gave a larger current density, indicating a better catalytic conversion of polysulfides.

The cycling stability of batteries using different separators was investigated by cycling performance tests. As shown in Fig. 4(d), the cell using the pristine PP separator shows an initial discharge capacity of 941.5 $\text{mAh}\cdot\text{g}^{-1}$ at 0.2 C. In contrast, the cells using the

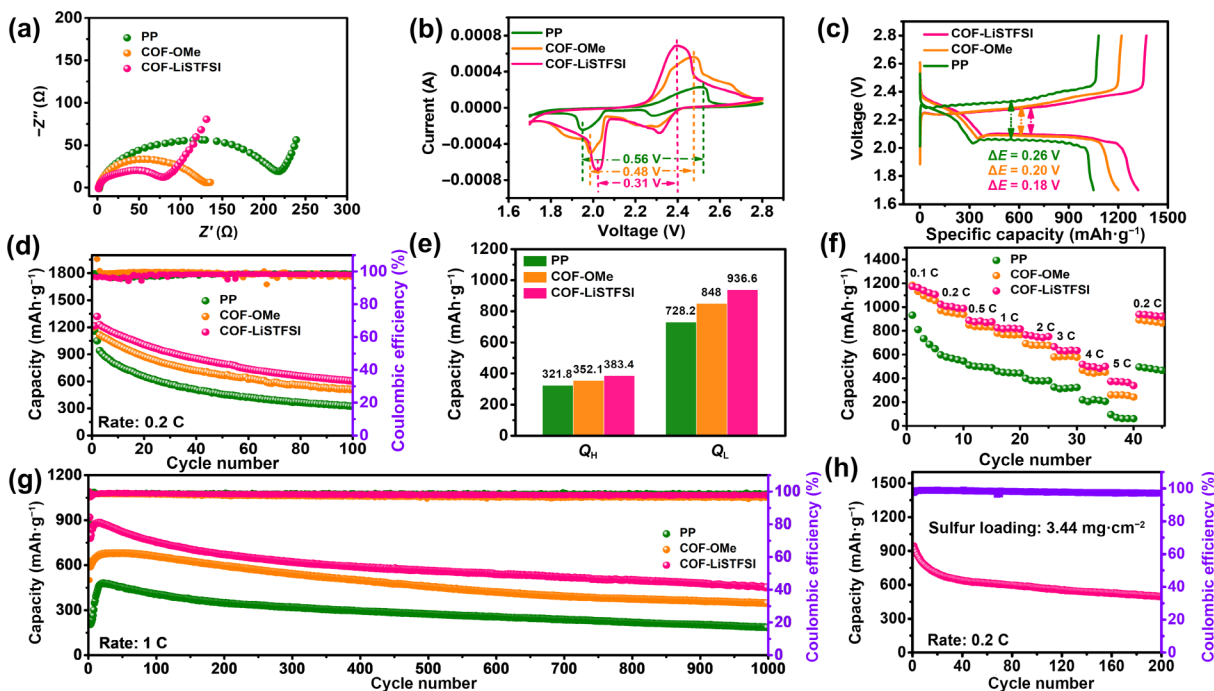


Figure 4 (a) EIS spectra of cells with different separators. (b) CV curves at $0.1 \text{ mV}\cdot\text{s}^{-1}$ of cells with different separators. (c) Charge–discharge voltage profiles of cells with different separators at 0.1 C . (d) Capacity retention performance of cells with different separators at 0.2 C . (e) Contribution of specific capacity to areas of high voltage and low voltage of cells with different separators. (f) Rate capability of cells with different separators. (g) Long-term cycling performance of cells with different separators at 1 C . (h) Cycling performance at 0.2 C of cell with COF-LiSTFSI separator with a high sulfur loading of $3.44 \text{ mg}\cdot\text{cm}^{-2}$.

COF-OMe and COF-LiSTFSI modified separators delivered enhanced initial discharge capacities of 1115.8 and $1229.7 \text{ mAh}\cdot\text{g}^{-1}$ at 0.2 C , respectively, indicating the higher utilization rate of the sulfur cathode. After 100 cycles, the cell using COF-LiSTFSI modified separator maintained a higher capacity of $606.7 \text{ mAh}\cdot\text{g}^{-1}$ than that of the cells using COF-OMe modified and the pristine PP separators. In the two-step discharge process (Fig. S22 in the ESM), there is a high-discharge plateau related to the formation of high-order soluble polysulfides and a low-discharge plateau reflecting the generation of insoluble Li_2S_2 and Li_2S . The capacity of high voltage (Q_H) represents the reversible electrochemical behavior ($2\text{Li}^+ + \text{S}_8 \leftrightarrow \text{Li}_2\text{S}_8$) and brings a relatively invariable capacity, and the practical promotion of capacity is mainly dependent on the enhanced performance in the region of low voltage (Q_L) [36]. Figure 4(e) is drawn for better understanding of the capacity in the areas of the Q_H and Q_L of cells with different separators. The cell with COF-LiSTFSI modified separator shows a higher capacity at the high-discharge plateau of $383.4 \text{ mAh}\cdot\text{g}^{-1}$, compared with the cells using pristine PP ($321.8 \text{ mAh}\cdot\text{g}^{-1}$) and COF-OMe ($352.1 \text{ mAh}\cdot\text{g}^{-1}$) modified separators. Additionally, the low-discharge plateau of the cell with COF-LiSTFSI modified separator exhibits superior capacity of $936.6 \text{ mAh}\cdot\text{g}^{-1}$, higher than that of the cells using PP ($728.2 \text{ mAh}\cdot\text{g}^{-1}$) and COF-OMe ($848.0 \text{ mAh}\cdot\text{g}^{-1}$) modified separators, indicating the higher conversion rate to solid $\text{Li}_2\text{S}_2/\text{Li}_2\text{S}$. Furthermore, the ratio between Q_L and Q_H of cell using COF-LiSTFSI modified separator is much higher than the cells using PP and COF-OMe modified separators and with the best retention rate (Fig. S23 in the ESM). The rate performances of the cells with different separators at various current rates from 0.1 to 5 C are compared in Fig. 4(f). Impressively, the rate performances of the cells using with both COF-OMe and COF-LiSTFSI modified separators exhibit higher capacities than that of the pristine PP separator, indicating the fast sulfur conversion kinetics of these COFs materials.

Other factors including long-term cycling stability and high sulfur loading should also be critically considered in practical

application [37]. The cycling performances of cells with different separators over 1000 cycles at 1 C were investigated (Fig. 4(g)). The cell with COF-LiSTFSI modified separator delivers a decent capacity of $884.5 \text{ mAh}\cdot\text{g}^{-1}$ and maintains a reversible capacity of $454.0 \text{ mAh}\cdot\text{g}^{-1}$ after 1000 cycles, with a low attenuation rate of 0.042% per cycle and an average Coulombic efficiency of 98.3% . In contrast, the cells with the pristine PP and COF-OMe modified separators exhibit low capacities ($480.1 \text{ mAh}\cdot\text{g}^{-1}$ for PP separator and $681.6 \text{ mAh}\cdot\text{g}^{-1}$ for COF-OMe modified separator, respectively) and poor attenuation rates (0.061% for PP separator and 0.049% for COF-OMe modified separator, respectively). To further evaluate practical application, a cathode with high sulfur loading of $3.44 \text{ mg}\cdot\text{cm}^{-2}$ was prepared using the COF-LiSTFSI modified separator. As illustrated in Fig. 4(h), the cell with COF-LiSTFSI modified separator exhibits an initial capacity of $944.1 \text{ mAh}\cdot\text{g}^{-1}$ and a remained capacity of $498.9 \text{ mAh}\cdot\text{g}^{-1}$ after 200 cycles at 0.2 C . Galvanostatic charge/discharge curves of batteries with high sulfur loading with different cycles are shown in Fig. S24 in the ESM. This indicates that the Li-S battery with COF-LiSTFSI modified separator has promising potential for commercial viability.

2.4 The diffusion coefficient of Li^+ (D_{Li^+}) of separators

To further confirm that the COF-LiSTFSI modified separator significantly facilitated Li^+ diffusion, the CV curves at varied scanning rates from 0.1 to $0.5 \text{ mV}\cdot\text{s}^{-1}$ were measured for investigating the Li^+ diffusion coefficient of different separators (Figs. 5(a)–5(c)). Note the certain change tendency between the peak current (I_p) and the scan rate (ν) and their functional relationship is as follows

$$I_p = (2.69 \times 10^5) n^{1.5} A D_{\text{Li}^+}^{0.5} C_{\text{Li}^+} \nu^{0.5} \quad (1)$$

where n is the number of transferred electrons, A is the contact area of active material, and C_{Li^+} is the ion concentration of electrolyte [38]. The fitting slope of I_p and $\nu^{0.5}$ in Eq. (1) can be used to determine the D_{Li^+} of separators in Li-S batteries under the same test conditions. After linear fitting of the scatter diagram in Fig. S25 in the ESM, the results of D_{Li^+} are compared in Fig. 5(d)

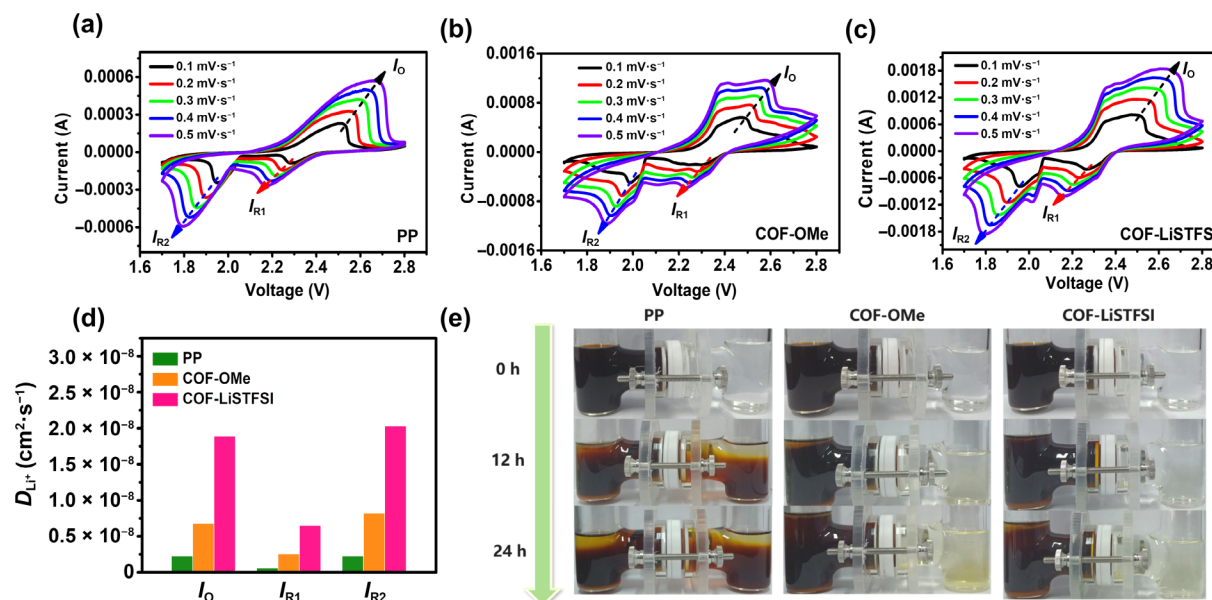


Figure 5 CV curves at different scan rates of cells with the (a) PP, (b) COF-OMe, and (c) COF-LiSTFSI modified separators. (d) D_{Li^+} of cells with different separators at different reaction stages. (e) Permeation experiments of PP, COF-OMe, and COF-LiSTFSI modified separators to Li_2S_6 solution for 0, 12, and 24 h.

and Table S2 in the ESM. Obviously, the COF-LiSTFSI separator exhibits the largest value of the diffusion coefficient at all the redox states (the oxidation peak current (I_O), the first reduction peak current (I_{R1}), and the second reduction peak current (I_{R2})), strongly confirming the significantly facilitated Li^+ diffusion behaviors by introducing lithium sulfonylimide group.

2.5 Permeation experiments of separators

To visually demonstrate the impediment ability toward polysulfides diffusion, the permeation experiments were performed using H-shaped cells with different separators (Fig. 5(e)). A 0.1 M Li_2S_6 solution with 1,3-dioxolane (DOL)/1,2-dimethoxyethan (DME) (v/v = 1:1) solvent was injected into one side of the separator, while the other side was injected with the blank solvent (DOL/DME (v/v = 1:1)). It was observed that the polysulfides easily diffused through the pristine PP separator within 12 h. On the contrary, in the cases of the COF-OMe and COF-LiSTFSI modified separators, there was almost no color change in the right chambers after 12 h. After 24 h, the right chamber of COF-LiSTFSI modified separator still showed no color change, while that of COF-OMe turned a little yellow. The excellent polysulfides blocking ability of the COF-LiSTFSI modified separator could be attributed to the synergistic effect of both physical barriers from nanopores of COFs and electrostatic interaction from the sulfonylimide anion group.

3 Conclusions

In summary, COF-LiSTFSI was designed and synthesized to modify the separator for Li-S batteries, providing a solution for addressing issues of polysulfides shuttle effect. The COF-LiSTFSI, with rich negatively charged sulfonylimide group, possesses both a high density of intrinsic charges and a highly ordered ion transportation pathway, which serve to facilitate Li^+ migration and repel polysulfide anions through electrostatic interaction. Consequently, the cells using COF-LiSTFSI modified separator exhibit a low attenuation rate of 0.042% per cycle over 1000 cycles at 1 C. When coupled with a high sulfur loading cathode of $3.44 \text{ mg}\cdot\text{cm}^{-2}$, a favorable initial capacity of $944.1 \text{ mAh}\cdot\text{g}^{-1}$ was achieved. This work establishes a new approach to tailor COF-modified separators with a lower shuttle effect and higher ion transport for high-performance Li-S batteries.

Acknowledgements

The authors gratefully acknowledge the financial support from the National Natural Science Foundation of China (No. 52090034) and the Higher Education Discipline Innovation Project (No. B12015).

Electronic Supplementary Material: Supplementary material (full details including materials and methods, characterizations, electrochemical measurements, calculation and computational methods, supplementary figures, and tables) is available in the online version of this article at <https://doi.org/10.1007/s12274-023-5683-1>.

References

- [1] Dunn, B.; Kamath, H.; Tarascon, J. M. Electrical energy storage for the grid: A battery of choices. *Science* **2011**, *334*, 928–935.
- [2] Albertus, P.; Babinec, S.; Litzelman, S.; Newman, A. Status and challenges in enabling the lithium metal electrode for high-energy and low-cost rechargeable batteries. *Nat. Energy* **2018**, *3*, 16–21.
- [3] Guo, X. T.; Xu, H. Y.; Li, W. T.; Liu, Y. Y.; Shi, Y. X.; Li, Q.; Pang, H. Embedding atomically dispersed iron sites in nitrogen-doped carbon frameworks-wrapped silicon suboxide for superior lithium storage. *Adv. Sci.* **2023**, *10*, 2206084.
- [4] Bruce, P. G.; Freunberger, S. A.; Hardwick, L. J.; Tarascon, J. M. $Li-O_2$ and $Li-S$ batteries with high energy storage. *Nat. Mater.* **2012**, *11*, 19–29.
- [5] Bhargava, A.; He, J. R.; Gupta, A.; Manthiram, A. Lithium-sulfur batteries: Attaining the critical metrics. *Joule* **2020**, *4*, 285–291.
- [6] Manthiram, A.; Fu, Y. Z.; Chung, S. H.; Zu, C. X.; Su, Y. S. Rechargeable lithium-sulfur batteries. *Chem. Rev.* **2014**, *114*, 11751–11787.
- [7] Pang, Q.; Liang, X.; Kwok, C. Y.; Nazar, L. F. Advances in lithium-sulfur batteries based on multifunctional cathodes and electrolytes. *Nat. Energy* **2016**, *1*, 16132.
- [8] Huang, S. Z.; Wang, Z. H.; Von Lim, Y.; Wang, Y.; Li, Y.; Zhang, D. H.; Yang, H. Y. Recent advances in heterostructure engineering for lithium-sulfur batteries. *Adv. Energy Mater.* **2021**, *11*, 2003689.
- [9] Chen, Y.; Wang, T. Y.; Tian, H. J.; Su, D. W.; Zhang, Q.; Wang, G. X. Advances in lithium-sulfur batteries: From academic research to commercial viability. *Adv. Mater.* **2021**, *33*, 2003666.
- [10] Chen, Z. X.; Zhao, M.; Hou, L. P.; Zhang, X. Q.; Li, B. Q.; Huang, J. Q. Toward practical high-energy-density lithium-sulfur pouch cells: A review. *Adv. Mater.* **2022**, *34*, 2201555.

- [11] Wang, M. L.; Song, Y. Z.; Sun, Z. T.; Shao, Y. L.; Wei, C. H.; Xia, Z.; Tian, Z. N.; Liu, Z. F.; Sun, J. Y. Conductive and catalytic VTe₂@MgO heterostructure as effective polysulfide promoter for lithium-sulfur batteries. *ACS Nano* **2019**, *13*, 13235–13243.
- [12] Xue, W. J.; Shi, Z.; Suo, L. M.; Wang, C.; Wang, Z. Q.; Wang, H. Z.; So, K. P.; Maurano, A.; Yu, D. W.; Chen, Y. M. et al. Intercalation-conversion hybrid cathodes enabling Li-S full-cell architectures with jointly superior gravimetric and volumetric energy densities. *Nat. Energy* **2019**, *4*, 374–382.
- [13] Xiao, W.; Kiran, G. K.; Yoo, K.; Kim, J. H.; Xu, H. Y. The dual-site adsorption and high redox activity enabled by hybrid organic-inorganic vanadyl ethylene glycolate for high-rate and long-durability lithium-sulfur batteries. *Small*, in press, <https://doi.org/10.1002/sml.202206750>.
- [14] Gao, X.; Zheng, X. L.; Wang, J. Y.; Zhang, Z. W.; Xiao, X.; Wan, J. Y.; Ye, Y. S.; Chou, L. Y.; Lee, H. K.; Wang, J. Y. et al. Incorporating the nanoscale encapsulation concept from liquid electrolytes into solid-state lithium-sulfur batteries. *Nano Lett.* **2020**, *20*, 5496–5503.
- [15] Li, S. L.; Zhang, W. F.; Zheng, J. F.; Lv, M. Y.; Song, H. Y.; Du, L. Inhibition of polysulfide shuttles in Li-S batteries: Modified separators and solid-state electrolytes. *Adv. Energy Mater.* **2021**, *11*, 2000779.
- [16] Jin, L. N.; Fu, Z. H.; Qian, X. Y.; Li, F.; Wang, Y. H.; Wang, B.; Shen, X. Q. Co-N/KB porous hybrid derived from ZIF 67/KB as a separator modification material for lithium-sulfur batteries. *Electrochim. Acta* **2021**, *382*, 138282.
- [17] Pang, Y.; Wei, J. S.; Wang, Y. G.; Xia, Y. Y. Synergetic protective effect of the ultralight MWCNTs/NCQDs modified separator for highly stable lithium-sulfur batteries. *Adv. Energy Mater.* **2018**, *8*, 1702288.
- [18] Lei, T. Y.; Chen, W.; Lv, W. Q.; Huang, J. W.; Zhu, J.; Chu, J. W.; Yan, C. Y.; Wu, C. Y.; Yan, Y. C.; He, W. D. et al. Inhibiting polysulfide shuttling with a graphene composite separator for highly robust lithium-sulfur batteries. *Joule* **2018**, *2*, 2091–2104.
- [19] Pei, F.; Lin, L. L.; Fu, A.; Mo, S. G.; Ou, D. H.; Fang, X. L.; Zheng, N. F. A two-dimensional porous carbon-modified separator for high-energy-density Li-S batteries. *Joule* **2018**, *2*, 323–336.
- [20] Jin, Z. Q.; Xie, K.; Hong, X. B.; Hu, Z. Q.; Liu, X. Application of lithiated Nafion ionomer film as functional separator for lithium sulfur cells. *J. Power Sources* **2012**, *218*, 163–167.
- [21] Ma, G. Q.; Huang, F. F.; Wen, Z. Y.; Wang, Q. S.; Hong, X. H.; Jin, J.; Wu, X. W. Enhanced performance of lithium sulfur batteries with conductive polymer modified separators. *J. Mater. Chem. A* **2016**, *4*, 16968–16974.
- [22] Jiao, L.; Zhang, C.; Geng, C. N.; Wu, S. C.; Li, H.; Lv, W.; Tao, Y.; Chen, Z. J.; Zhou, G. M.; Li, J. et al. Capture and catalytic conversion of polysulfides by *in situ* built TiO₂-MXene heterostructures for lithium-sulfur batteries. *Adv. Energy Mater.* **2019**, *9*, 1900219.
- [23] Luo, Y. F.; Luo, N. N.; Kong, W. B.; Wu, H. C.; Wang, K.; Fan, S. S.; Duan, W. H.; Wang, J. P. Multifunctional interlayer based on molybdenum diphosphide catalyst and carbon nanotube film for lithium-sulfur batteries. *Small* **2018**, *14*, 1702853.
- [24] Ghazi, Z. A.; He, X.; Khattak, A. M.; Khan, N. A.; Liang, B.; Iqbal, A.; Wang, J. X.; Sin, H.; Li, L. S.; Tang, Z. Y. MoS₂/Celgard separator as efficient polysulfide barrier for long-life lithium-sulfur batteries. *Adv. Mater.* **2017**, *29*, 1606817.
- [25] Hong, X. J.; Song, C. L.; Yang, Y.; Tan, H. C.; Li, G. H.; Cai, Y. P.; Wang, H. X. Cerium based metal-organic frameworks as an efficient separator coating catalyzing the conversion of polysulfides for high performance lithium-sulfur batteries. *ACS Nano* **2019**, *13*, 1923–1931.
- [26] Song, C. L.; Li, G. H.; Yang, Y.; Hong, X. J.; Huang, S.; Zheng, Q. F.; Si, L. P.; Zhang, M.; Cai, Y. P. 3D catalytic MOF-based nanocomposite as separator coatings for high-performance Li-S battery. *Chem. Eng. J.* **2020**, *381*, 122701.
- [27] Chen, C.; Jiang, Q. B.; Xu, H. F.; Zhang, Y. P.; Zhang, B. K.; Zhang, Z. Y.; Lin, Z.; Zhang, S. Q. Ni/SiO₂/graphene-modified separator as a multifunctional polysulfide barrier for advanced lithium-sulfur batteries. *Nano Energy* **2020**, *76*, 105033.
- [28] Yan, W. Q.; Gao, X. W.; Yang, J. L.; Xiong, X. S.; Xia, S.; Huang, W.; Chen, Y. H.; Fu, L. J.; Zhu, Y. S.; Wu, Y. P. Boosting polysulfide catalytic conversion and facilitating Li⁺ transportation by ion-selective COFs composite nanowire for Li-S batteries. *Small* **2022**, *18*, 2106679.
- [29] Jiang, C.; Tang, M.; Zhu, S. L.; Zhang, J. D.; Wu, Y. C.; Chen, Y.; Xia, C.; Wang, C. L.; Hu, W. P. Constructing universal ionic sieves via alignment of two-dimensional covalent organic frameworks (COFs). *Angew. Chem., Int. Ed.* **2018**, *57*, 16072–16076.
- [30] Cao, Y.; Wu, H.; Li, G.; Liu, C.; Cao, L.; Zhang, Y. M.; Bao, W.; Wang, H. L.; Yao, Y.; Liu, S. et al. Ion selective covalent organic framework enabling enhanced electrochemical performance of lithium-sulfur batteries. *Nano Lett.* **2021**, *21*, 2997–3006.
- [31] Cao, Y.; Liu, C.; Wang, M. D.; Yang, H.; Liu, S.; Wang, H. L.; Yang, Z. X.; Pan, F. S.; Jiang, Z. Y.; Sun, J. Lithiation of covalent organic framework nanosheets facilitating lithium-ion transport in lithium-sulfur batteries. *Energy Storage Mater.* **2020**, *29*, 207–215.
- [32] Xu, J.; An, S. H.; Song, X. Y.; Cao, Y. J.; Wang, N.; Qiu, X.; Zhang, Y.; Chen, J. W.; Duan, X. L.; Huang, J. H. et al. Towards high performance Li-S batteries via sulfonate-rich COF-modified separator. *Adv. Mater.* **2021**, *33*, 2105178.
- [33] Gao, J. Y.; Wang, C.; Han, D. W.; Shin, D. M. Single-ion conducting polymer electrolytes as a key jigsaw piece for next-generation battery applications. *Chem. Sci.* **2021**, *12*, 13248–13272.
- [34] Li, X. L.; Zhang, C. L.; Cai, S. L.; Lei, X. H.; Altoe, V.; Hong, F.; Urban, J. J.; Ciston, J.; Chan, E. M.; Liu, Y. Facile transformation of imine covalent organic frameworks into ultrastable crystalline porous aromatic frameworks. *Nat. Commun.* **2018**, *9*, 2998.
- [35] Fang, R. P.; Zhao, S. Y.; Sun, Z. H.; Wang, D. W.; Cheng, H. M.; Li, F. More reliable lithium-sulfur batteries: Status, solutions, and prospects. *Adv. Mater.* **2017**, *29*, 1606823.
- [36] Li, Y. J.; Lin, S. Y.; Wang, D. D.; Gao, T. T.; Song, J. W.; Zhou, P.; Xu, Z. K.; Yang, Z. H.; Xiao, N.; Guo, S. J. Single atom array mimic on ultrathin MOF nanosheets boosts the safety and life of lithium-sulfur batteries. *Adv. Mater.* **2020**, *32*, 1906722.
- [37] Zhao, M.; Li, B. Q.; Zhang, X. Q.; Huang, J. Q.; Zhang, Q. A perspective toward practical lithium-sulfur batteries. *ACS Cent. Sci.* **2020**, *6*, 1095–1104.
- [38] Wang, L.; Zhang, Y. M.; Guo, H. Y.; Li, J.; Stach, E. A.; Tong, X.; Takeuchi, E. S.; Takeuchi, K. J.; Liu, P.; Marschilok, A. C. et al. Structural and electrochemical characteristics of Ca-doped “flower-like” Li₄Ti₃O₁₂ motifs as high-rate anode materials for lithium-ion batteries. *Chem. Mater.* **2018**, *30*, 671–684.